Applied Catalysis B: Environmental 138–139 (2013) 167–174

Contents lists available at SciVerse ScienceDirect

Applied Catalysis B: Environmental

journal homepage: www.elsevier.com/locate/apcatb

Green synthesis and catalytic properties of polyallylamine functionalized tetrahedral palladium nanocrystals

Gengtao Fu, Xian Jiang, Linfei Ding, Lin Tao, Yu Chen*, Yawen Tang, Yiming Zhou, Shaohua Wei, Jun Lin*, Tianhong Lu

Jiangsu Key Laboratory of New Power Batteries, Laboratory of Electrochemistry, College of Chemistry and Materials Science, Nanjing Normal University, 1# Wenyuan Road, Nanjing 210023, PR China

ARTICLE INFO

Article history:
Received 17 October 2012
Received in revised form 21 February 2013
Accepted 27 February 2013
Available online 6 March 2013

Keywords:
Green synthesis
Polyallylamine
Palladium nanocrystals
Tetrahedra
Catalytic activity

ABSTRACT

The water-soluble polyallylamine (PAH) functionalized tetrahedral palladium nanocrystals with adjustable size and concavity are successfully achieved through a one-pot hydrothermal synthesis. The size, morphology and surface composition of tetrahedral palladium nanocrystals are investigated by transmission electron microscopy (TEM), high angle annular dark field scanning TEM (HAADF-STEM), selected area electron diffraction (SAED), X-ray diffraction (XRD), fourier transform infrared (FT-IR) and X-ray photoelectron spectroscopy (XPS). The anchorage of PAH on palladium nanocrystals results in excellent colloidal stability and anti-oxidation capability of palladium nanocrystals. Both {1 1 0} and {1 1 1}-enclosed concave tetrahedral palladium nanocrystals (*c*-Pd-TNCs) exhibit superior catalytic activity to only {1 1 1}-enclosed flat tetrahedral palladium nanocrystals (*f*-Pd-TNCs) for the hydrogenation reduction of nitro functional groups and C=N double bond.

1. Introduction

Palladium nanostructures have attracted considerable attention due to their potential applications in many fields such as heterogeneous catalysis [1–7], hydrogen storage/sensing [8–10] and electrocatalysis [11–19], etc. By tailoring the size and/or shape, one can enhance their catalytic performance in a range of applications, originating from the size and/or facet effects. Palladium nanocrystals with various morphologies, such as wires [13,20,21], spheres [16,22,23], springs [24], tubes [25], belts [26], cubes [27], tetrahexahedra [28], plates [29], cubooctahedra [30], octahedra [2,31], tetrahedra [32], concave cubes [33,34] and concave tetrahedra [35], have been synthesized by different methods such as templating, seeding, electrodeposition, polyol process and thermal decomposition, etc. Among various synthesis methods, the solution-phase chemical reduction method has emerged as a highly versatile and powerful tool for the large-scale and size/shape-controlled synthesis of the single crystalline palladium nanostructures.

The kinetically controlled synthesis of the palladium nanocrystals has advanced remarkably in organic solution (such as ethylene glycol, benzyl alcohol and dimethyl formamide) containing surfactants (such as polyvinyl pyrrolidone and tetradecyltrimethylammonium bromide) [29,30,32,35,36]. Compared to the synthesis in organic system, a water-based system provides a more environmentally benign route for the synthesis of metal nanocrystals, because it doesn't involve toxic organic solvent [37]. Till now, the synthesis of the single crystalline palladium nanostructures with uniform size and well-defined shape in aqueous solution has still been at an initial stage [2,20].

During the synthesis of noble metal nanostructures, the synthetic polymers were generally employed to stabilize noble metal nanostructures [38], which limited aggregation of the metal nanoparticles, and imparted catalytic selectivity by restricting access to active sites [39]. Polyallylamine hydrochloride (PAH, shown in Supplementary data, Scheme S1), a positively charged polyelectrolytes, contains a large number of primary amine groups in a molecule and has excellent hydrophilic property. Previous investigations indicated the positively charged amine groups in PAH readily bound the negatively charged $PdCl_4^{2-}$ ion in acidic conditions through the electrostatic interaction [40–43]. Very recently, we found that PAH could interact with $PdCl_2$ to generate the colorless PAH-Pd^{II} complex in basic conditions, similar to the case of $[Pd^{II}(NH_3)_4]^{2-}$ ion [16]. By using the PAH-Pd^{II} complex as reaction precursor and hydrazine hydrate as reductant, the PAH functionalized porous palladium nanospheres were achieved conveniently under mild reaction conditions (35 °C), and the PAH functionalized porous palladium nanospheres possessed high catalytic activity and good stability for the Mizoroki–Heck reaction [16]. Herein we report a simple and green method for the high-yield synthesis of tetrahedral palladium nanocrystals with adjustable size and

* Corresponding authors. Tel.: +86 25 85891651; fax: +86 25 83243286.
E-mail addresses: ndchenyu@yahoo.cn (Y. Chen), linjun@njnu.edu.cn (J. Lin).

0926-3373/$ – see front matter © 2013 Elsevier B.V. All rights reserved.
http://dx.doi.org/10.1016/j.apcatb.2013.02.052

concavity through a one-pot hydrothermal method, with PAH as complex-forming agent, capping agent and facet-selective agent, and formaldehyde as reductant.

2. Experimental

2.1. Reagents and chemicals

Polyallylamine hydrochloride (PAH, weight-average molecular weight 15,0000, shown in Scheme S1) was supplied from Nitto Boseki Co., Ltd. (Tokyo, Japan). Palladium chloride ($PdCl_2$), formaldehyde solution (HCHO, 40%), sodium borohydride ($NaBH_4$), 4-nitrophenol and methylene blue were purchased from Sinopharm Chemical Reagent Co., Ltd. (Shanghai, China). Other reagents were of analytical reagent grade and used without further purification. All the aqueous solutions were prepared with Millipore water having a resistivity of 18.2 MΩ. The solution pH was adjusted by the addition of dilute NaOH or HCl solution.

2.2. Synthesis of tetrahedral palladium nanocrystals

In a typical synthesis, 1 mL of 0.1 M $PdCl_2$ and 1.7 mL of 0.52 M PAH (molarity of PAH given with respect to the repeating unit) were added into 16.7 mL of water with continued stirring (molar ratio of PAH monomer to Pd^{II} was 9:1 [16]). After adjusting solution pH to 9.0 (Similar to the case of $[Pd^{II}(NH_3)_4]Cl_2$ in $PdCl_2$-$NH_3{\cdot}H_2O$ system, PAH can interact with $PdCl_2$ to generate colorless PAH-Pd^{II} complex by coordination to the amine groups in basic conditions) [16], 0.5 mL of formaldehyde solution (40%) was added into the homogeneous colorless solution. Then, the colorless mixture was transferred to a 50-mL Teflon-lined stainless-steel autoclave, and was then heated at 120 °C for 4 hours. After being cooled to room temperature, the obtained flat tetrahedral palladium nanocrystals (*f*-Pd-TNCs) were separated by centrifugation at 15,000 rpm for 10 min, washed several times with water, and then dried at 60 °C for 5 h in a vacuum dryer. Under the same other conditions, the effects of temperature, feeding ratio of PAH/Pd^{II}, feeding ratio of HCHO/Pd^{II} and reaction time on morphological features were also investigated.

2.3. Physical characterization

Ultraviolet and visible spectroscopy (UV–vis) was recorded at room temperature on a Shimadzu UV3600 spectrophotometer equipped with 1.0 cm quartz cells. X-ray diffraction (XRD) patterns were obtained with Model D/max-rC X-ray diffractometer using Cu K_a radiation source (λ = 1.5406 Å) and operating at 40 kV and 100 mA. Transmission electron microscopy (TEM) was made on a JEOL JEM-2100F transmission electron microscopy operated at an accelerating voltage of 200 kV. X-ray photoelectron spectroscopy (XPS) was performed with a Thermo VG Scientific ESCALAB 250 spectrometer with a monochromatic Al Ka X-ray source, and the vacuum in the analysis chamber was maintained at about 10^{-9} mbar. The binding energy was calibrated by means of the C 1s peak energy of 284.6 eV. Fourier transform infrared (FT-IR) was carried out using a Nicolet 520 SXFTIR spectrometer. The spectra were collected in the wave number range between 400 and 4000 cm^{-1} over 128 scans at a resolution of 4 cm^{-1}. The zeta potential measurements were performed with a Malvern Zetasizer Nano ZS90 analyzer at room temperature. The pH measurements were carried out using a METTLER TOLEDO DETTA320 Digital pH-meter.

All electrochemical experiments were carried out on a CHI 660 C electrochemical workstation (CH Instruments, Shanghai Chenghua Co.). A standard three-electrode system was used for all electrochemical experiments, which consisted of a platinum wire as the auxiliary electrode, a saturated calomel reference electrode, and a catalyst modified glassy carbon electrode as the working electrode. Potentials in this study were reported with respect to the reversible hydrogen electrode (RHE). The catalyst dispersions were prepared by mixing a certain amount of catalyst with appropriate amount of water. A designed amount of dispersion was drop-cast onto the surface of the pretreated glassy carbon electrode. After drying the electrode at room temperature, 2.5 μL of 5.0 wt.% Nafion solution was spread on the surface of the catalyst layer and allowed to dry. The palladium metal loading on the electrode surface was about 4 μg. Cyclic voltammetry (CV) measurements were conducted in N_2-saturated 0.5 M H_2SO_4 aqueous solution. All of the electrochemical measurements were carried out at room temperature.

2.4. Catalytic reduction of 4-nitrophenol

The catalytic reduction of 4-nitrophenol to 4-aminophenol was studied by UV–vis employing previously described methods. Typically, 0.5 mL of 0.1 M $NaBH_4$ and 2 mL of 1×10^{-4} M 4-nitrophenol solutions were first put in a quartzy cuvette having 1-cm path length. Then, 40 μL of tetrahedral palladium nanocrystals aqueous solution (0.4 g L^{-1}) was added into the mixture solution. The progress of the conversion of 4-nitrophenol to 4-aminophenol was then monitored by recording the time-dependent absorption spectra of the reaction system at a regular time interval of 1 min.

2.5. Catalytic reduction of methylene blue

Typically, 0.5 mL of 0.1 M $NaBH_4$ and 2 mL of 5×10^{-5} M methylene blue solutions were first put in a quartzy cuvette having 1-cm path length. Then, 5 μL of tetrahedral palladium nanocrystals aqueous solution (0.4 g L^{-1}) was added into the mixture solution. The reduction progress of methylene blue was then monitored by recording the time-dependent absorption spectra of the reaction system at a regular time interval of 1 min.

3. Results and discussion

3.1. Characterization of tetrahedral palladium nanocrystals

In a typical synthesis, 1.0 mL of 0.1 M $PdCl_2$ and 1.7 mL of 0.52 M PAH were added into 16.7 mL water. After adjusting solution pH to 9.0, 0.5 mL of formaldehyde solution (40%) was added into the colorless PAH-Pd^{II} complex solution. After heating at 120 °C for 4 h, the flat tetrahedral palladium nanocrystals (*f*-Pd-TNCs) were obtained (see Section 2 for details). The representative TEM and high angle annular dark field scanning TEM (HAADF-STEM) images of the as-prepared palladium nanoparticles were shown in Fig. 1A–B. As observed, the *f*-Pd-TNCs enclosed by four {1 1 1} facet [44] are the dominant products with a typical yield of >75% and a side length of 25 ± 4 nm. High-resolution TEM (HRTEM, Fig. 1C–D), SAED (insert in Fig. 1C) and XRD (Supplementary data, Fig. S1) measurements clearly indicate their single-crystalline nature and face centered cubic structure. It is worth noting that the PAH and formaldehyde in centrifugate can be reutilized (*noting*: the oxidation–reduction reaction between PAH and Pd^{II} species cann't occur under the present experimental conditions). After supplementary addition of 1 mL of 0.1 M $PdCl_2$, 0.1 mL of 0.52 M PAH and 0.2 mL of formaldehyde solution (40%) to centrifugate, the *f*-Pd-TNCs can be re-obtained under the identical experimental conditions (i.e., pH 9.0, 120 °C) (Supplementary data, Fig. S2). Such recycling is particularly attractive in terms of "Green Chem.".

To explore the formation process of the *f*-Pd-TNCs, UV-vis was firstly used to monitor the reaction process momentarily (Fig. 2). In the initial stage of reaction, the characteristic peak of PAH-Pd^{II}

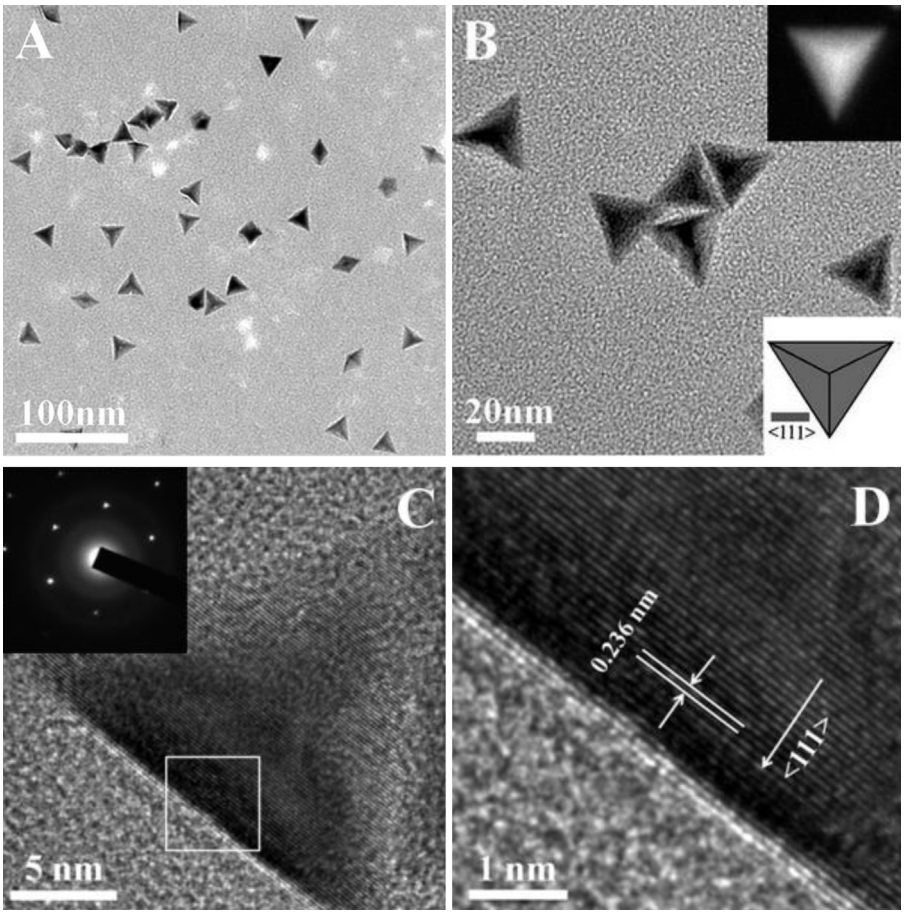

Fig. 1. Representative (A) large-area and (B) enlarged TEM images of as-synthesized *f*-Pd-TNCs. Top-right and bottom-right inserts show the corresponding HAADF-STEM image of an individual *f*-Pd-TNCs and the ideal structure model of the flat palladium tetrahedron, respectively. (C) HRTEM image of an individual *f*-Pd-TNCs. Insert shows the corresponding SAED pattern of as-synthesized *f*-Pd-TNCs. (D) HRTEM image of the squared area indicated in (C).

complex at 215 nm decreases slowly in intensity with time, accompanying the appearance of localized surface plasmon resonance of palladium nanoparticles (i.e., the very wide UV absorption in the wavelength range of 800–190 nm). After 120 min, the absorbance value of reaction solution reaches a maximum value and remains almost invariable, which is indicative of the formation of palladium nanoparticles with well-defined shape.

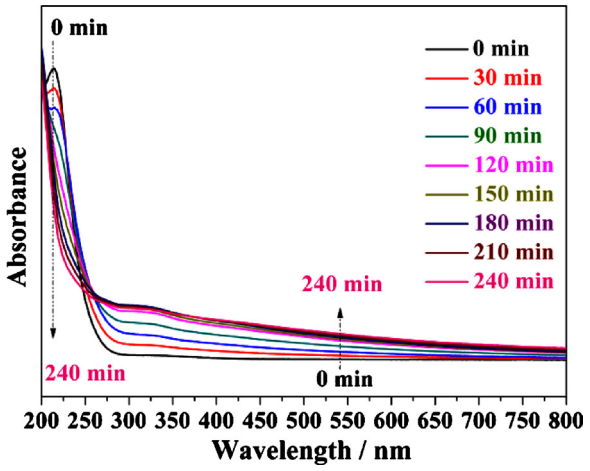

Fig. 2. UV–vis absorption spectra of the reaction system at different stages.

The morphological evolution of the palladium nanocrystals with the reaction time was further investigated by TEM (Fig. 3 and Supplementary data, Fig. S3). The *f*-Pd-TNCs produced in a 30-min reaction have a side length of ~10 nm. Their average side length increase to ~18 nm at 1 h, and ~25 nm at 2 h. Beyond 2 h, no further change on both the size and morphology of palladium nanocrystals is observed, in accordance with the above UV–vis data. These results demonstrate that the *f*-Pd-TNCs are developed at the very beginning and concomitant with the growth process [35].

In the present PAH-Pd^{II} complex/formaldehyde system, the morphology of the palladium nanocrystals was independent on the reaction temperature. The reactions under the same conditions but at lower temperature yields the *f*-Pd-TNCs with a smaller particle size (Supplementary data, Fig. S4). The particle size of the *f*-Pd-TNCs can also be controlled by the concentration of formaldehyde. When the amount of formaldehyde solution (40%) is reduced from 5.0 to 0.1 mL, the particle size of the *f*-Pd-TNCs decreases from 35 to 17 nm (Fig. 4A–C and Supplementary data, Fig. S5). It is noteworthy that reducing the amount of formaldehyde to 0.05 mL results in the formation of palladium tetrapod nanocrystals (yield of >50%, Fig. 4D and Supplementary data, Fig. S5D). For the palladium tetrapod nanocrystals, further controlled synthesis is in progress.

Noble-metal nanocrystals with a concave structure on the surface have physical/chemical properties different from those enclosed by a flat or convex surface [45]. Interestingly, it was found that the feeding ratio of PAH/Pd^{II} controlled the morphology of palladium nanocrystals. Increasing the feeding ratio of PAH/Pd^{II} to 40:1 produces the concave tetrahedral palladium nanocrystals

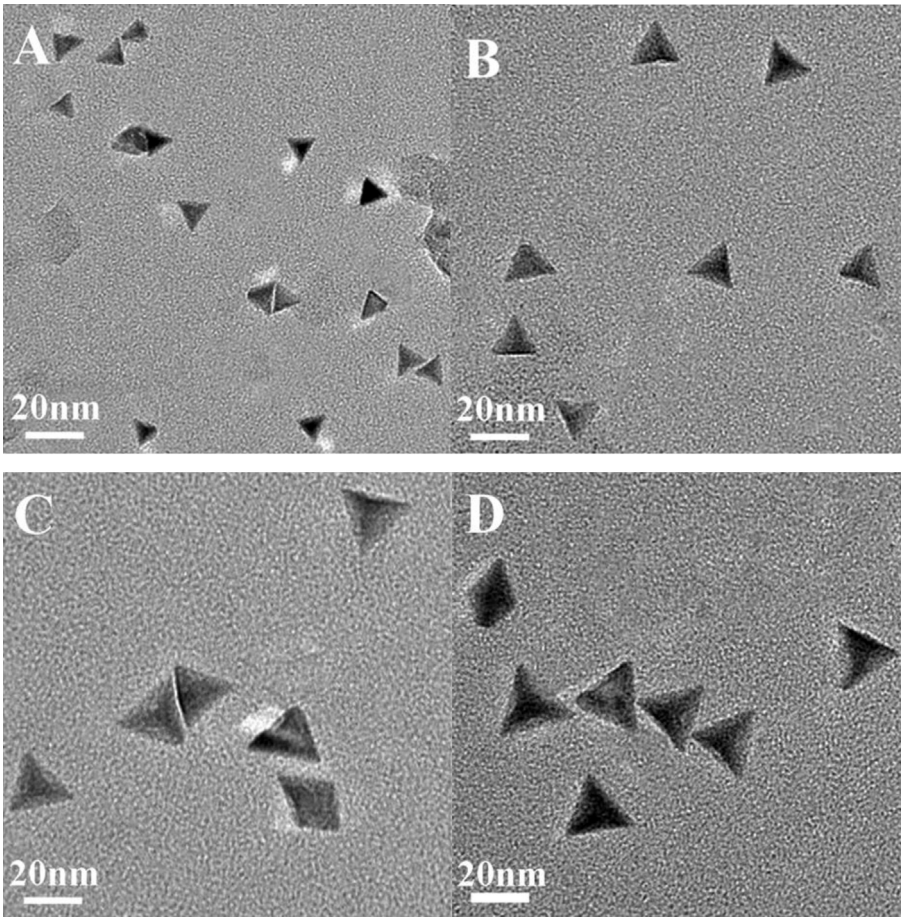

Fig. 3. TEM images of the tetrahedral palladium nanocrystals produced in (A) 0.5, (B) 1.0, (C) 2.0 and (D) 4.0 h reaction time.

(*c*-Pd-TNCs) with side length of 32 ± 3 nm (Fig. 5A–B). The concave feature is also confirmed by the HAADF-STEM image (insert in Fig. 5B). Further SAED (insert in Fig. 5C) and XRD (Supplementary data, Fig. S6) patterns indicate the *c*-Pd-TNCs have also single-crystalline nature and face centered cubic structure. According to the ideal structure model of the concave palladium tetrahedron reported by Prof. Zheng (insert in Fig. 5B), each *c*-Pd-TNCs consists of four {1 1 1} faces shaped in a hollow equilateral triangle and 12 isosceles trianglelike {1 1 0} faces concave toward the center of the tetrahedron [35]. As observed, the appearance of palladium {1 1 0} faces confirms as-prepared products are the concave tetrahedral palladium nanocrystals (Fig. 5D). Under thermodynamic control of strong chemisorption, the roles of formaldehyde and amines in the shape control of noble metal nanocrystals had been widely investigated and discussed [46]. Similar to the case of amine-assisted synthesis of Pt nanocrystals with high-index facet [47], the emergence of high energy palladium {1 1 0} facet [48] in the *c*-Pd-TNCs may arise from the contribution of the coordination adsorption of amine groups when the supplied PAH is larger than a certain amount, owing to the likely competitive adsorption of PAH and formaldehyde on palladium crystal surface. Further detailed investigations on the formation mechanism of *c*-Pd-TNCs are in progress.

Homogeneous catalytic systems generally exhibit better activity and selectivity than heterogeneous systems. For the large-scale applications in liquid phase reactions, however, heterogeneous catalysts have many advantages over homogeneous counterparts, including easy removal from reaction mixtures and catalyst recyclability [23]. In recent, homogeneous catalysis on palladium nanoparticles homogeneously dispersed in water have attracted much attention due to its nature of green and sustainable chemistry [49]. In the present synthesis system, PAH molecules anchor effectively to the surface of tetrahedral palladium nanocrystals (see FT-IR data in Supplementary data, Fig. S7; *noting*: here only take *f*-Pd-TNCs as an example in the whole paragraph because the spectral and electrochemical data of the *f*-Pd-TNCs are identical with the *c*-Pd-TNCs, Fig. S8), resulting in excellent colloidal stability of the tetrahedral palladium nanocrystals in water (i.e., no precipitation was observed in 3 months, Fig. S9). It is well known that the higher zeta potential of nanoparticles corresponds to the higher surface charge density of nanoparticles, which generally make the nanoparticles suspensions maintain a higher stability due to electrical repulsion. The high zeta potential of tetrahedral palladium nanocrystals ($+25 \pm 5$ mV) and the hydrophilic property of PAH molecules are responsible for excellent colloidal stability. Meanwhile, it is observed that binding energy values of Pd^0 and $Pd^{II}O$ species in tetrahedral palladium nanocrystals negatively shifted ca. 0.6 eV compared to that of palladium nanoparticles (termed Pd-control) obtained by the controlled experiment without PAH (Fig. 6). Further cyclic voltammetry measurements indicate the as-prepared tetrahedral palladium nanocrystals have excellent anti-oxidation capability (Fig. 7). As observed, a pronounced oxidation-reduction peak of palladium occurs at the Pd-control nanoparticles, but no obviously electrochemical response is observed at the as-prepared tetrahedral palladium nanocrystals in the potential range from 0.4 to 1.0 V. The d-band center theory has indicated that lowering of the d-band

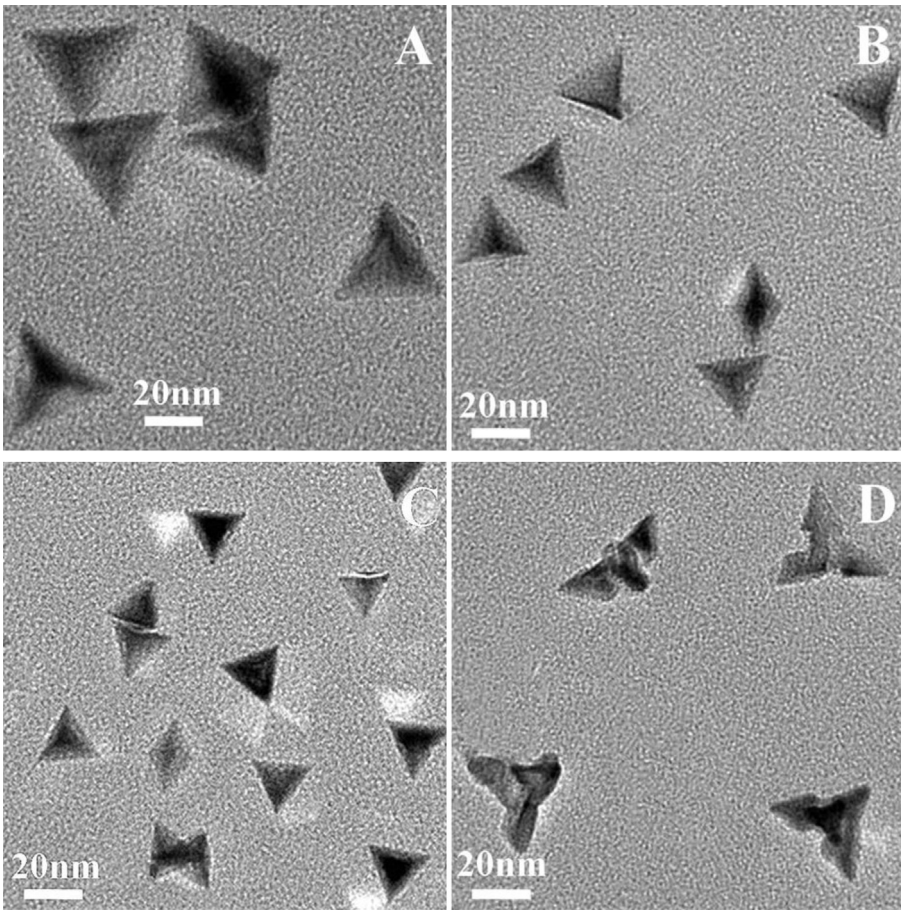

Fig. 4. TEM images of palladium nanocrystals prepared at different formaldehyde amount. (A) 5.0; (B) 0.5; (C) 0.1 and (D) 0.05 mL.

center results in the decrease in interaction strength of the various adsorbates to the substrate [50,51]. Thus, the sharply negative shift of binding energy of palladium atom results in a very weak oxophilicity of tetrahedral palladium nanocrystals. Overall, the change of the electronic structure of palladium atom and surface cover of PAH at palladium nanocrystals surface are responsible for excellent anti-oxidation capability of the as-prepared tetrahedral palladium nanocrystals. We also performed accelerated oxidation tests by placing 5 mg of Pd-control nanoparticles and *f*-Pd-TNCs in 5 mL of 0.05 M HNO_3 solution at 60 °C. It is observed that the Pd-control nanoparticles and *f*-Pd-TNCs dissolve completely at 20 min and 160 min, respectively, indicating anti-oxidation capability of the PAH functionalized tetrahedral palladium nanocrystals is seven times bigger than that of the Pd-control nanoparticles. Obviously, excellent anti-oxidation capability of as-prepared tetrahedral palladium nanocrystals improves their catalytic stability in further practice applications.

3.2. Catalytic activity

Palladium-catalyzed reduction of nitro groups to amines has been extensively investigated due to its importance in wastewater treatment and organic synthesis [52–55]. Since the reduction of 4-nitrophenol by $NaBH_4$ occurred directly on the metallic surface [56–58], the reduction reaction was studied as a model reaction to probe the facet-dependent catalytic activity of palladium nanoparticles by using *f*-Pd-TNCs (25 nm) and *c*-Pd-TNCs (32 nm) as catalysts. The Pd-catalyzed reduction of 4-nitrophenol was monitored using time-resolved UV–vis spectra, and a detailed kinetic analysis was performed [58]. As shown in Fig. 8A, upon the introduction of the palladium nanocrystals to the reaction solution, the peak of 4-nitrophenol at 400 nm decreases rapidly with time, accompanying with the gradual emergence of a new peak at 300 nm corresponding to the formation of 4-aminophenol. After reduction, the peak of 4-nitrophenol at 400 nm completely vanished, indicating the conversion of p-nitrophenol is nearly 100%. Although the particle size of *c*-Pd-TNCs (32 nm) is bigger than *f*-Pd-TNCs (25 nm), the reduction of 4-nitrophenol to 4-aminophenol is finished within 9 min with *c*-Pd-TNCs (Fig. 8A) while that 14 min with *f*-Pd-TNCs (Fig. 8B). From the monitoring of the consumption of the nitro reagent as a function of time, the pseudo-first-order rate constant of the reaction on *f*-Pd-TNCs and *c*-Pd-TNCs are calculated to be 0.17 min^{-1} and 0.29 min^{-1} (Supplementary data, Fig. S10), indicating palladium {1 1 0} facet with high energy [48] was more active than palladium {1 1 1} facet with low energy for 4-nitrophenol reduction. For comparison, the catalytic activity of the Pd-control nanoparticles for the reduction of 4-nitrophenol was also investigated (Supplementary data, Fig. S11). The reduction of 4-nitrophenol to 4-aminophenol is finished within 44 min. Obviously, the catalytic activities of the PAH functionalized tetrahedral palladium nanocrystals are much better than that of the Pd-control nanoparticles, which may be ascribed to excellent dispersibility of the PAH functionalized tetrahedral palladium nanocrystals in water. To further evaluate the catalytic performance of the tetrahedral palladium nanocrystals, the turnover frequencies (TOF, defined as the number of 4-nitrophenol molecules per metallic Pd per minute based on the total mass of metallic Pd, the unit is $mol^1\ mol^{-1}\ min^{-1}$) of *c*-Pd-TNCs and

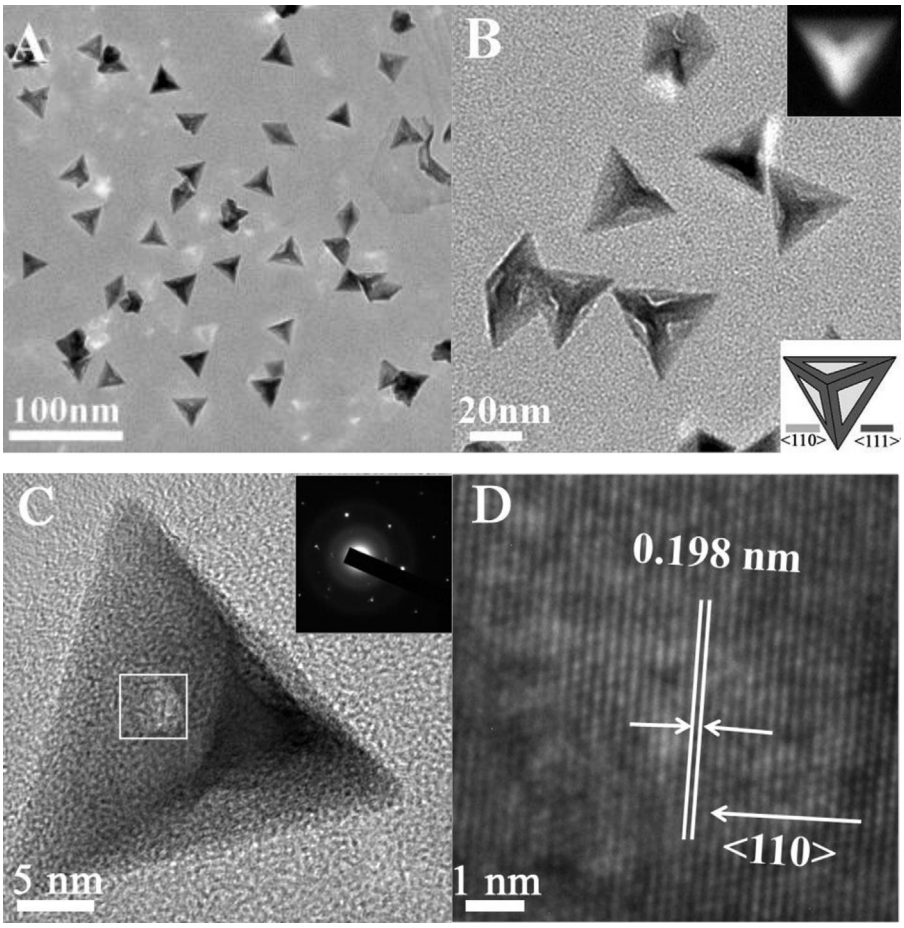

Fig. 5. Representative (A) large-area and (B) enlarged TEM images of as-synthesized *c*-Pd-TNCs. Top-right and bottom-right inserts show the corresponding HAADF-STEM image of an individual *c*-Pd-TNCs and the ideal structure model of the concave palladium tetrahedron, respectively. (C) HRTEM image of an individual *c*-Pd-TNCs. Insert shows the corresponding SAED pattern of as-synthesized *c*-Pd-TNCs. (D) HRTEM image of the squared area indicated in (C).

f-Pd-TNCs were calculated to be 0.148 and 0.095 $mol^1\ mol^{-1}\ min^{-1}$, respectively (the correlative experimental parameters see Section 2). In comparison with the recently reported mesoporous silica coated Au heterogeneous catalyst (0.042 $mol^1\ mol^{-1}\ min^{-1}$ of TOF) [59], and hollow Pd/Fe_3O_4 spheres (0.015 $mol^1\ mol^{-1}\ min^{-1}$ of TOF) and solid Pd/Fe_3O_4 spheres (0.01 $mol^1\ mol^{-1}\ min^{-1}$ of TOF) [55], the PAH functionalized tetrahedral palladium nanocrystals show more competitive catalytic activity. After selecting the reduction of methylene blue as a model reaction, UV–vis investigations demonstrate the catalytic activity of *c*-Pd-TNCs is also better than that of *f*-Pd-TNCs (Supplementary data, Fig. S12), indicating that palladium {1 1 0} facet is also more active than palladium {1 1 1} facet for the hydrogenation reduction of C=N double bond.

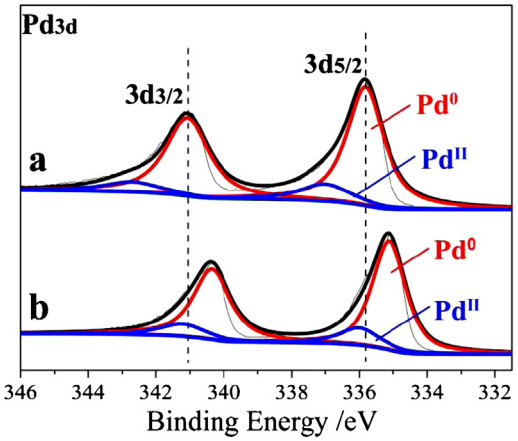

Fig. 6. XPS spectra of (a) Pd-control nanoparticles and (b) *f*-Pd-TNCs in the Pd 3d region.

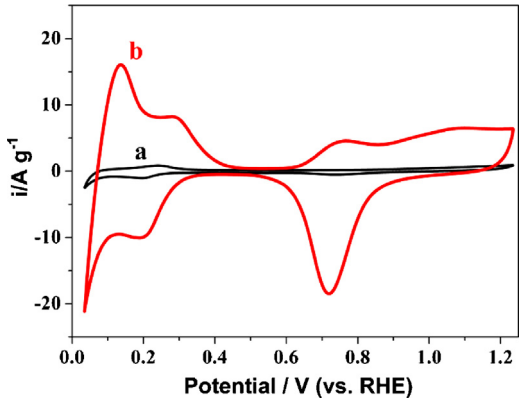

Fig. 7. Cyclic voltammograms of (a) *f*-Pd-TNCs and (b) Pd-control nanoparticles in 0.1 M $HClO_4$ solution at the rate of 50 mV s^{-1}.

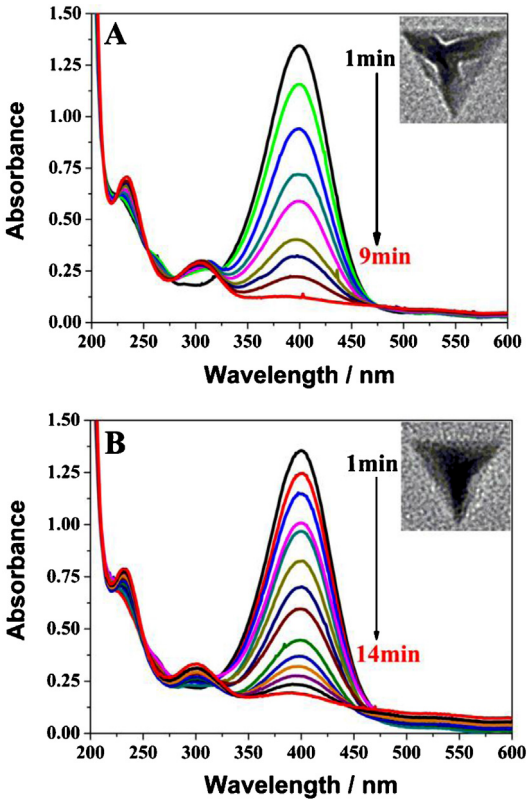

Fig. 8. UV–vis spectra for the reduction of 4-nitrophenol measured at 1 min intervals using (A) *c*-Pd-TNCs and (B) *f*-Pd-TNCs. Conditions: [4-nitrophenol] = 8.0×10^{-5} M; [Pd] = 6.4 mg L^{-1}; [$NaBH_4$] = 0.02 M.

4. Conclusions

In summary, we report a simple and green method to synthesize the water-soluble PAH functionalized tetrahedral palladium nanocrystals with adjustable size and concave degree. The anchorage of PAH on palladium nanocrystals results in excellent colloidal stability and anti-oxidation capability of palladium nanocrystals. Thanks to the facet effect, the *c*-Pd-TNCs exhibit much superior catalytic activity for the reduction of 4-nitrophenol and methylene blue than the *f*-Pd-TNCs. With the advantages of enhanced catalytic activity, high durability, and simple fabrication, the obtained PAH functionalized tetrahedral palladium nanocrystals are very promising for applications in energy- and catalysis-related areas. Since PAH can also interact with M^{II} ion (M = Cu^{II}, Pt^{II} and Ag^{I}) to generate the PAH-M^{II} complex, the present PAH-M^{II} system can also be used to synthesize other M (M = Cu, Pt and Ag) nanocrystals.

Acknowledgments

This work was supported by NSFC (21073094 and 21273116), the United Fund of NSFC and Yunnan Province (U1137602), Industry-Academia Cooperation Innovation Fund Project of Jiangsu Province (BY2012001), and a project funded by the Priority Academic Program Development of Jiangsu Higher Education Institutions.

Appendix A. Supplementary data

Supplementary data associated with this article can be found, in the online version, at http://dx.doi.org/10.1016/j.apcatb.2013.02.052.

References

[1] A. Modak, A. Deb, T. Patra, S. Rana, S. Maity, D. Maiti, Chemical Communications 48 (2012) 4253–4255.
[2] M. Crespo-Quesada, A. Yarulin, M. Jin, Y. Xia, L. Kiwi-Minsker, Journal of the American Chemical Society 133 (2011) 12787–12794.
[3] L.M. Gomez-Sainero, X.L. Seoane, A. Arcoya, Applied Catalysis B: Environmental 53 (2004) 101–110.
[4] J. Jung, S. Bae, W. Lee, Applied Catalysis B: Environmental 127 (2012) 148–158.
[5] R. Zhang, H. Liu, B. Wang, L. Ling, Applied Catalysis B: Environmental 126 (2012) 108–120.
[6] W. Sun, Q. Li, S. Gao, J.K. Shang, Applied Catalysis B: Environmental 125 (2012) 1–9.
[7] S. Li, Y.L. Fang, C.D. Romanczuk, Z. Jin, T. Li, M.S. Wong, Applied Catalysis B: Environmental 125 (2012) 95–102.
[8] J. Zou, K.S. Iyer, C.L. Raston, Green Chemistry 14 (2012) 906–908.
[9] M. Moreno, F.J. Ibanez, J.B. Jasinski, F.P. Zamborini, Journal of the American Chemical Society 133 (2011) 4389–4397.
[10] X.Q. Zeng, M.L. Latimer, Z.L. Xiao, S. Panuganti, U. Welp, W.K. Kwok, T. Xu, Nano Letters 11 (2011) 262–268.
[11] Y. Xu, R. Xu, J. Cui, Y. Liu, B. Zhang, Chemical Communications 48 (2012) 3881–3883.
[12] Y. Dai, X. Mu, Y. Tan, K. Lin, Z. Yang, N. Zheng, G. Fu, Journal of the American Chemical Society 134 (2012) 7073–7080.
[13] C. Koenigsmann, A.C. Santulli, E. Sutter, S.S. Wong, ACS Nano 5 (2011) 7471–7487.
[14] M. Zheng, P. Li, G. Fu, Y. Chen, Y. Zhou, Y. Tang, T. Lu, Applied Catalysis B: Environmental 129 (2013) 394–402.
[15] Y. Liang, Y. Zhou, J. Ma, J.Y. Zhao, Y. Chen, Y.W. Tang, T.H. Lu, Applied Catalysis B: Environmental 103 (2011) 388–396.
[16] G. Fu, W. Han, L. Yao, J. Lin, S. Wei, Y. Chen, Y. Tang, Y. Zhou, T. Lu, X. Xia, Journal of Materials Chemistry 22 (2012) 17604–17611.
[17] C. Jimenez-Borja, S. Brosda, F. Matei, M. Makri, B. Delgado, F. Sapountzi, D. Ciuparu, F. Dorado, J.L. Valverde, C.G. Vayenas, Applied Catalysis B: Environmental 128 (2012) 48–54.
[18] M.H. Seo, S.M. Choi, J.K. Seo, S.H. Noh, W.B. Kim, B. Han, Applied Catalysis B: Environmental 129 (2013) 163–171.
[19] G. Zhang, Y. Wang, X. Wang, Y. Chen, Y. Zhou, Y. Tang, L. Lu, J. Bao, T. Lu, Applied Catalysis B: Environmental 102 (2011) 614–619.
[20] X. Huang, N. Zheng, Journal of the American Chemical Society 131 (2009) 4602–4603.
[21] F. Yang, S.C. Kung, M. Cheng, J.C. Hemminger, R.M. Penner, ACS Nano 4 (2010) 5233–5244.
[22] L. Zhang, J.W. Zhang, Z.Y. Jiang, S.F. Xie, M.S. Jin, X.G. Han, Q. Kuang, Z.X. Xie, L.S. Zheng, Journal of Materials Chemistry 21 (2011) 9620–9625.
[23] S.W. Kim, M. Kim, W.Y. Lee, T. Hyeon, Journal of the American Chemical Society 124 (2002) 7642–7643.
[24] L. Liu, S.H. Yoo, S.A. Lee, S. Park, Nano Letters 11 (2011) 3979–3982.
[25] L. Liu, S. Park, Chemistry of Materials 23 (2011) 1456–1460.
[26] M.N. Nadagouda, V. Polshettiwar, R.S. Varma, Journal of Materials Chemistry 19 (2009) 2026–2031.
[27] D. Hao, S.X. Zhao, S.C. Min, H. Chao, X.Z. Chuan, L. Chen, T. Yuan, W.D. Ke, G.H. Jun, Chinese Physics B 19 (2010) 106104.
[28] N. Tian, Z.Y. Zhou, N.F. Yu, L.Y. Wang, S.G. Sun, Journal of the American Chemical Society 132 (2010) 7580–7581.
[29] Y. Xiong, J.M. McLellan, J. Chen, Y. Yin, Z.Y. Li, Y. Xia, Journal of the American Chemical Society 127 (2005) 17118–17127.
[30] Y. Xiong, J. Chen, B. Wiley, Y. Xia, S. Aloni, Y. Yin, Journal of the American Chemical Society 127 (2005) 7332–7333.
[31] W. Niu, L. Zhang, G. Xu, ACS Nano 4 (2010) 1987–1996.
[32] H. Zhu, G. Li, Q. Chi, Y. Zhao, H. Liu, J. Li, T. Huang, CrystEngCommunity 14 (2012) 1531–1533.
[33] M. Jin, H. Zhang, Z. Xie, Y. Xia, Angewandte Chemie International Edition 50 (2011) 7850–7854.
[34] Y.L. Qin, X.B. Zhang, J. Wang, L.M. Wang, Journal of Materials Chemistry 22 (2012) 14861–14863.
[35] X.Q. Huang, S.H. Tang, H.H. Zhang, Z.Y. Zhou, N.F. Zheng, Journal of the American Chemical Society 131 (2009) 13916–13917.
[36] H. Lee, S.E. Habas, G.A. Somorjai, P. Yang, Journal of the American Chemical Society 130 (2008) 5406–5407.
[37] B. Lim, X. Lu, M. Jiang, P.H.C. Camargo, E.C. Cho, E.P. Lee, Y. Xia, Nano Letters 8 (2008) 4043–4047.
[38] L.D. Rampino, F.F. Nord, Journal of the American Chemical Society 63 (1941) 2745–2749.
[39] H. Li, Z.H. Zhu, J. Liu, S.H. Xie, H.X. Li, Journal of Materials Chemistry 20 (2010) 4366–4370.
[40] B. Liu, H. Li, L. Die, X. Zhang, Z. Fan, J. Chen, Journal of Power Sources 186 (2009) 62–66.
[41] M.R. Regan, I.A. Banerjee, Scripta Materialia 54 (2006) 909–914.
[42] Y. Hong, A. Sen, Chemistry of Materials 19 (2007) 961–963.
[43] A. Wołowicz, Z. Hubicki, Chemical Engineering Journal 174 (2011) 510–521.
[44] A.X. Yin, X.Q. Min, Y.W. Zhang, C.H. Yan, Journal of the American Chemical Society 133 (2011) 3816–3819.
[45] H. Zhang, M. Jin, J. Wang, W. Li, P.H.C. Camargo, M.J. Kim, D. Yang, Z. Xie, Y. Xia, Journal of the American Chemical Society 133 (2011) 6078–6089.
[46] M. Chen, B.H. Wu, J. Yang, N.F. Zheng, Advanced Materials 24 (2012) 862–879.

[47] X. Huang, Z. Zhao, J. Fan, Y. Tan, N. Zheng, Journal of the American Chemical Society 133 (2011) 4718–4721.
[48] D. Wang, H.L. Xin, H. Wang, Y. Yu, E. Rus, D.A. Muller, F.J. DiSalvo, H.D. Abruña, Chemistry of Materials 24 (2012) 2274–2281.
[49] H. Zhang, Y. Yang, W. Dai, D. Yang, S. Lu, Y. Ji, Catalysis Science & Technology 2 (2012) 1319–1323.
[50] B. Hammer, J. Nørskov, Surface Science 343 (1995) 211–220.
[51] M. Mavrikakis, B. Hammer, J.K. Nørskov, Physical Review Letters 81 (1998) 2819–2822.
[52] J. Shui, J.C.M. Li, Nano Letters 9 (2009) 1307–1314.
[53] R. Chen, Y. Jiang, W. Xing, W. Jin, Angewandte Chemie International Edition 50 (2011) 4405–4411.
[54] V. Komanicky, H. Iddir, K.C. Chang, A. Menzel, G. Karapetrov, D. Hennessy, P. Zapol, H. You, Journal of the American Chemical Society 131 (2009) 5732–5733.
[55] H.Q. Wang, X. Wei, K.X. Wang, J.S. Chen, Dalton Transactions 41 (2012) 3204–3208.
[56] J. Zhang, G. Chen, M. Chaker, F. Rosei, D. Ma, Applied Catalysis B: Environmental 132–133 (2013) 107–115.
[57] S. Behrens, A. Heyman, R. Maul, S. Essig, S. Steigerwald, A. Quintilla, W. Wenzel, J. Burck, O. Dgany, O. Shoseyov, Advanced Materials 21 (2009) 3515–3519.
[58] R. Bhandari, M.R. Knecht, Langmuir 28 (2012) 8110–8119.
[59] Y. Deng, Y. Cai, Z. Sun, J. Liu, C. Liu, J. Wei, W. Li, C. Liu, Y. Wang, D. Zhao, Journal of the American Chemical Society 132 (2010) 8466–8473.